Evaluation of Thermal Neutron Scattering Law and Cross Sections for Calcium Hydride

Briana K. Laramee[1], *Ayman* I. Hawari[1]

[1]Department of Nuclear Engineering, North Carolina State University, Raleigh, NC 27695, USA

Abstract. Presented here are the calculated thermal scattering law (TSL) and thermal neutron scattering cross sections for Calcium Hydride, hereafter referred to by its chemical symbol CaH_2. The only other such data prior to this evaluation are thermal neutron scattering libraries in the JEFF database, which suffer from nonphysical features and inaccuracies. The data in this evaluation are calculated from first principles; Density Functional Theory (DFT) is used to calculate the phonon density of states (DOS), which is the primary input required to calculate the TSL. The TSL and cross sections have been evaluated for the three non-equivalent atom cites in the CaH_2: Ca, H_1, and H_2. Each evaluation has been submitted to the NNDC for consideration in the next ENDF/B release.

1 Introduction

CaH_2 is being considered for use as a moderator in new reactor designs, including a small modular microreactor [1]. Metal hydrides have long been known to be effective moderators based on various properties; ZrH_2 has been successfully used in TRIGA reactors for decades. Of crucial importance to the moderating behavior of any material, especially for use in thermal reactors, is the thermal neutron scattering mechanism. Unlike higher-energy cross sections which are determined empirically, thermal neutron scattering cross sections can be derived from first principles [2], [3]. This means that these cross sections can be calculated for any material, and are not limited by the availability of experimental data. This paper describes the process of evaluating new thermal scattering data for CaH_2.

2 Thermal Scattering Theory

The double-differential scattering cross section is related to the probability of a neutron scattering from incident energy E into outgoing energy dE' about E', through solid angle dΩ about Ω. The derived form is shown in Eq. 1, where k_B is the Boltzmann constant; T is the absolute temperature (K); σ_{coh} and σ_{inc} are the bound coherent and incoherent neutron scattering cross sections (b), respectively; and $S(\alpha,\beta)$ is the TSL.

$$\frac{\partial^2\sigma}{\partial\Omega\partial E'} = \frac{1}{4\pi k_B T}\sqrt{\frac{E}{E'}}[\sigma_{coh}S(\alpha,\beta) + \sigma_{inc}S_S(\alpha,\beta)] \quad (1)$$

The TSL is inherently a material property; it is the Fourier transform of the time-dependent pair correlation function in both space and time. It describes the probability distribution of the energy and momentum states of the material, and thus defines how a thermal neutron may interact with the scattering system. It is comprised of two components, as shown in Eq. 2; the distinct component (S_d) contains interatomic interference effects while the self-component (S_s) does not.

$$S(\alpha,\beta) = S_s(\alpha,\beta) + S_d(\alpha,\beta) \quad (2)$$

The incoherent approximation assumes that the contribution of S_d is negligible to the total TSL ($S_d = 0$), and thus the TSL is entirely incoherent. For crystalline materials the harmonic approximation allows the TSL to be calculated via a phonon expansion, which requires the phonon DOS. This DOS can be calculated via density functional theory (DFT), which is a method of calculating material properties using a quantum-mechanical model of electron density, in combination with lattice dynamics analysis.

3 Computational Method

CaH_2 has an orthorhombic crystal structure with symmetry described by the *Pnma* space group (#62). Its unit cell contains three non-equivalent (not related by symmetry) atom sites, labelled in this work as Ca, H_1, and H_2; Figure 3 shows the CaH_2 unit cell. The structural information was fed to the Vienna *ab initio* Simulation Package (VASP) [4], [5] which performs the DFT calculations, and the MedeA-VASP [6] platform was used to perform a structure optimization. The *ab initio* lattice dynamics (AILD) DFT calculation was initiated using the projector-augmented wave (PAW) method [7] and a GGE-PBE exchange-correlation functional. The structure optimization informed a plane-wave cut-off energy of 675eV and a 9x9x9 Monkhorst-Pack k-point mesh. VASP and PHONON [8], [9] are used to calculate the Hellmann-Feynman forces and subsequently the

phonon dispersion curves and DOS using the dynamical matrix method.

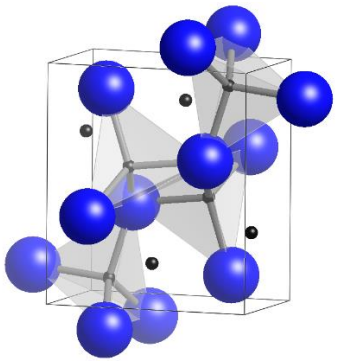

Fig. 1. CaH_2 unit cell. The large spheres are Ca; the small spheres H. The H_1 coordination polyhedra are shown.

4 Results

The results of the structure optimization are shown below in Table 1. The lattice constants show excellent agreement with experimental data [10]. This data was used to calculate the phonon DOS shown in Figure 2. The DOS has three sets of clustered peaks, corresponding to each of the non-equivalent atoms; the low-energy acoustic modes belong to the high-mass Ca atom and the high-energy optical modes to the H atoms (the more tightly-bound H_1 modes are the higher-energy of the two optical groups). These are compared on a one-to-one basis, and to experimental data [11]. The experimental data is naturally weighted towards the energy states of the H atoms; no attempt was made to undo the experimental weighting or apply it to the calculated data. The portion of the DOS which has the most significant impact on thermal neutron scattering is the beginning of each mode, which will always be occupied regardless of temperature. As temperature increases, so do the occupied energy levels, and hence the energies available to the thermal neutrons increases. These crucial regions of the DOS well match the experimental curves.

Table 1. Comparison of calculated to experimental CaH_2 lattice constants.

Lattice Constant	This Work	Experiment	Error (%)
a (Å)	5.92176	5.92852	0.114
b (Å)	3.57607	3.57774	0.0468
c (Å)	6.78272	6.78956	0.1007

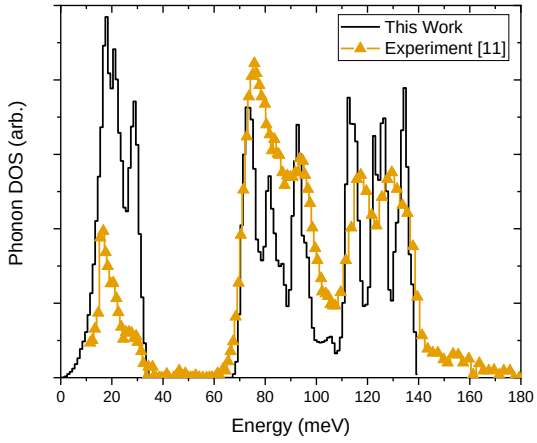

Fig 2. Comparison between the calculated phonon DOS and experiment.

The existing thermal neutron scattering cross sections in the JEFF libraries [12] suffer from several severe problems, specifically in the evaluation of Ca in CaH_2. Table 2 shows the bound coherent and incoherent neutron scattering cross sections of Ca and H, taken from the NIST database (note that these are not necessarily the values used in this work; they are shown for explanatory purposes). It is clear based on these data that Ca is almost entirely a coherent scatterer while H is almost entirely an incoherent scatterer. However, the JEFF evaluation only includes the incoherent component of the Ca cross section and overestimates it by several orders of magnitude. This can be seen in Figure 3 below, where the horizontal line is the bound incoherent scattering cross section. Additionally, the behavior of the unique H sites are averaged in the JEFF evaluation, which results in lost information.

Table 2. Bound coherent (σ_b^{coh}) and incoherent (σ_b^{inc}) neutron scattering cross sections for Ca and H from NIST

Isotope	σ_b^{coh} [b]	σ_b^{inc} [b]
Ca (natural)	2.64	0.000675
^{1}H	1.7568	80.26

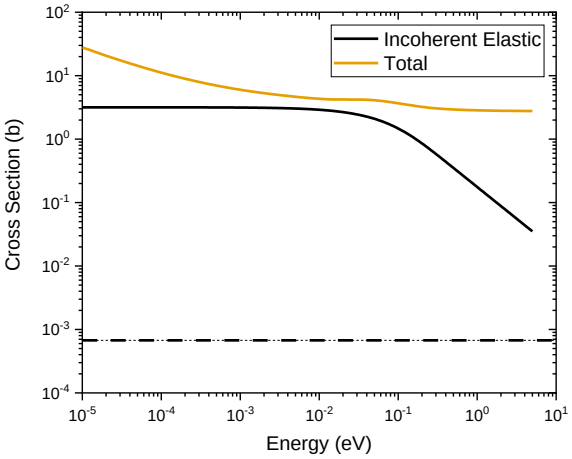

Fig 3. Components of the Ca in CaH_2 cross section in the JEFF libraries. The dashed horizontal line is the bound incoherent cross section, to which the incoherent elastic cross section should asymptote at low energies.

The phonon DOS was passed to the *FLASSH* code [13], where a 500-order phonon expansion was used to calculate the TSL using the cubic approximation. The code also calculated the incoherent inelastic cross section for all three non-equivalent atoms, the coherent elastic (cubic approximation) for Ca, and the incoherent elastic for H_1 and H_2. Figure 4 is a comparison between the total Ca cross sections of this work and of the JEFF libraries. Figure 5 shows the total cross section of H_1 at various temperatures as calculated in this work (the H_2 cross sections have similar features shifted to lower energies). Finally, Figure 6 is an analysis of the calculated H_1 cross section compared to Fermi's prediction for the interaction between a neutron and H in a hydrogenous substance [14]. There is shown to be great agreement with the predicted phenomena; as the mass of the binding atom increases, the data approaches

Fermi's values for an effectively infinite binding mass. The shift in peak energies relative to Fermi's calculation indicated anharmonicity in the lattice vibrations of both hydrides. The ZrH_2 data was generated for this comparison and closely matches both experimental [15] and recent AILD data [16]. The hydride data are normalized such that the first local minima are aligned with Fermi's data.

5 Conclusions

The thermal scattering law and cross sections of CaH_2 were calculated using *ab initio* methods. The data were generated for each of the three non-equivalent sites in CaH_2: Ca, H_1, and H_2. The cross sections for each are consistent with the physics of the scattering system – the contributions to Ca in CaH_2 are incoherent inelastic and coherent elastic, while the contributions for H_1 and H_2 are incoherent inelastic and incoherent elastic. This is an improvement over the existing data in the JEFF-3.3 database, particularly for the Ca cross section. The TSLs and cross sections generated in this work have been submitted to the NNDC for consideration in the next ENDF database release, ENDF/B-VIII.1.

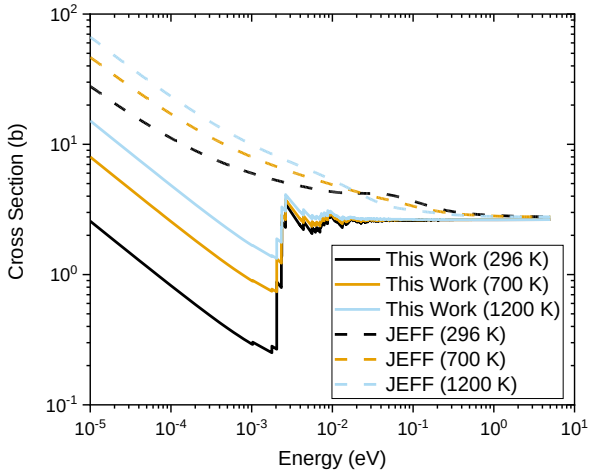

Fig 4. Comparison of total cross sections of Ca in CaH_2 from this work (solid) and JEFF (dashed).

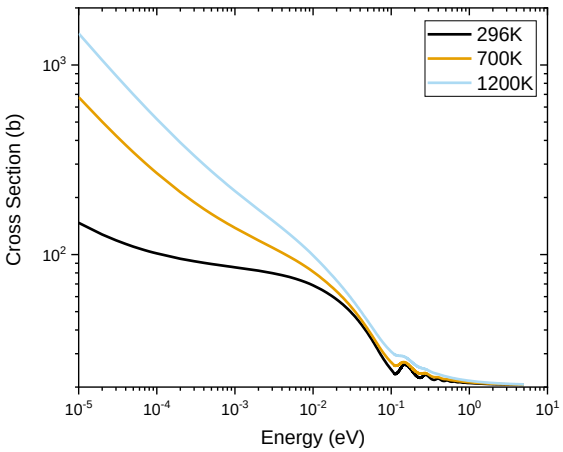

Fig 5. Total cross sections for H_1 in CaH_2 as calculated in this work for several temperatures.

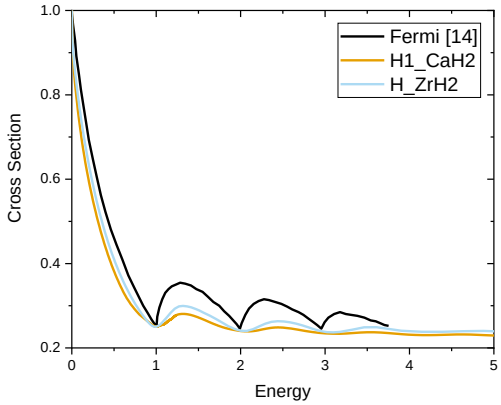

Fig 6. Comparison between the thermal neutron scattering cross section in a hydrogenous material as derived by Fermi [14], and the calculated cross section for H_1 in CaH_2 at 296K and H in ZrH_2 at 296K.

This work was partially funded by the US National Nuclear Security Administration's (NNSA) Nuclear Criticality Safety Program (NCSP), and the US Naval Nuclear Propulsion Program (NNPP).

References

[1] R. Kimura and S. Wada, *Nuclear Science and Engineering*, **193**, 9, p. 1013–1022 (2019).

[2] A. I. Hawari, *Nuclear Data Sheets*, **118**, 1, p. 172–175 (2014).

[3] A. I. Hawari, et al., *Ab Initio Generation of Thermal Neutron Scattering Cross Sections,* in Proceedings of PHYSOR, The Physics of Fuel Cycles and Advanced Nuclear Systems : Global Development, Chicago, IL (2004).

[4] G. Kresse and J. Furthmüller, *Computational Materials Science*, **6**, 1, p. 15–50 (1996).

[5] G. Kresse and J. Furthmüller, *Physical Review B*, **54**, 16, p. 11169 (1996).

[6] "MedeA," software, Version 3.0

[7] G. Kresse and D. Joubert, *Physical Review B*, **59**, 3, p. 1758 (1999).

[8] K. Parlinski, Z. Q. Li, and Y. Kawazoe, *Physical Review Letters*, **78**, 21, p. 4063 (1997).

[9] K. Parlinski, "PHONON." Cracow (2013).

[10] H. Wu, W. Zhou, T. J. Udovic, J. J. Rush, and T. Yildirim, *Journal of Alloys and Compounds*, **436**, 1–2, p. 51–55 (2007).

[11] P. Morris, D. K. Ross, S. Ivanov, D. R. Weaver, and O. Serot, *Journal of Alloys and Compounds*, **363**, 1–2, p. 88–92 (2004).

[12] O. Serot, in *AIP Conference Proceedings*, **769**, 1, p. 1446–1449 (2005).

[13] Zhu. Y and A. I. Hawari, "Full Law Analysis Scattering System Hub (FLASSH)" (2018).

[14] E. Fermi, *La Ricerca Scientifica*, **2**, 13 (1936).

[15] W. L. Whittemore, *Neutron Interactions in Zirconium Hydride; GA-4490*, San Diego, CA (1964).

[16] J. Wormald, M. Zerkle, and J. Holmes, *Journal of Nuclear Engineering*, **2**, p. 105–113 (2021).